Environmental Research 240 (2024) 117401

Contents lists available at ScienceDirect

Environmental Research

journal homepage: www.elsevier.com/locate/envres

Highly sensitive resistance spectroscopy technique for online monitoring of biofilm growth on metallic surfaces

Zoi Christina Kampouraki [a], Maria Petala [b], Konstantinos Zacharias [a], Avraam Konstantinidis [c], Xenophon Zabulis [d], Polykarpos Karamaounas [d], Margaritis Kostoglou [a], Thodoris D. Karapantsios [a,*]

[a] Division of Chemical Technology, School of Chemistry, Aristotle University of Thessaloniki, University Box 116, 541 24, Thessaloniki, Greece
[b] Department of Civil Engineering, Aristotle University of Thessaloniki, 541 24, Thessaloniki, Greece
[c] Laboratory of Engineering Mechanics, School of Civil Engineering, Aristotle University of Thessaloniki, GR, 541 24, Thessaloniki, Greece
[d] Institute of Computer Science, Foundation for Research and Technology, 711 10, Heraklion, Greece

ARTICLE INFO

Keywords:
Biofilms
Online monitoring
Electrical resistance spectroscopy
Biofilm thickness
Flow cell

ABSTRACT

Online techniques for monitoring biofilm formation and evolution are limited, especially as regards its application in flowing water systems. This is chiefly due to the absence of efficient non-destructive and non-invasive sensing methods. In this study, a sensitive electrical resistance spectroscopy technique is developed to monitor non-invasively and in real time the growth of biofilms over metallic surfaces inside water flow systems. To this aim, *Pseudomonas fluorescens* strain is used for biofilm development lasting 72 h in a laboratory-scale test channel of orthogonal cross section. Biofilm development corresponds to a progressively increasing coverage of the metallic surface area up to full coverage and a progressively increasing thickness. Biofilm development is registered by continuous recording of electrical impedance signals (time series). Proper configuration and tuning of the electronics promote the resistive contribution to the signal whereas careful grounding diminishes electrical interferences and yields superb sensing sensitivity. An increase of relative electrical resistance of around 15% is noticed in 72 h flow experiments which is attributed to both an increase of metallic surface area coverage and an increase of biofilm thickness. An independent estimation of these quantities using imaging tools and microscopy analysis, indicates that full coverage of the metallic surface occurs after only 48 h of the flow experiment, whereas biofilm thickness increases gradually along the entire 72 h of the experiment. Cross-examination of electrical signals with biofilm characteristics (metallic surface coverage and biofilm thickness) reveals that, qualitatively speaking, electrical signals are rather more sensitive to metallic surface coverage than biofilm thickness.

1. Introduction

World Health Organization guidelines state that human health should be protected by any microorganism in drinking water that might pose a threat (WHO, 2002). In water distribution systems (WDS), biofilms are the predominant form of bacteria that can form inside the pipes, acting as reservoirs for pathogenic microbial contaminants (Liu et al., 2016). Bacterial biofilms are dynamic and complex structures that respond to the external environment (Yin et al., 2019). Compared to planktonic life of bacteria, biofilms are defined as three dimensional bacterial aggregates, embedded in a complex matrix of extracellular polymeric substances (EPS), attached irreversibly to biotic and abiotic surfaces (Cloete et al., 2009; Costerton, 1999). EPS is composed of proteins, polysaccharides, extracellular DNA, glycolipids and nucleic acids (Hall-Stoodley et al., 2004), conferring a structure with an established resistance to disinfectants and antimicrobial treatments (Ceri et al., 1999). As pathogenic bacteria become more prevalent, infections and environmental problems caused by them will represent a major health and environmental concern (European Centre for Disease Prevention and Control-European Medicines Agency, 2009). Many chronic bacterial infections are caused by biofilms because they increase bacterial pathogens' resistance to antibiotics, resulting in lasting chronic infections (Costerton et al., 1999). Like so, biofilms are a cause of deterioration of water quality in WDS, biocorrosion and biofouling in

* Corresponding author.
E-mail address: karapant@chem.auth.gr (T.D. Karapantsios).

https://doi.org/10.1016/j.envres.2023.117401
Received 3 August 2023; Received in revised form 2 October 2023; Accepted 11 October 2023
Available online 31 October 2023

industrial water systems pipes (Beech and Sunner, 2004; LeChevallier et al., 1987), while also affect the alteration of organoleptic characteristics (taste, odor, color) (Prest et al., 2016).

It is widely acknowledged that the formation and resilience of biofilms inside water distribution systems' pipes remains one of the most challenging problems. It is therefore urgent to develop an appropriate and effective strategy to monitor biofilm formation. So far, analytical tools for easy and convenient online and real-time monitoring of the biofilm formation process have been scarce, as most of the available techniques related to the study and evaluation of the already formed biofilm are destructive and, thus, not allowing the corresponding substrate to be further analyzed.

At present, biofilm monitoring generally involves various analytical methods. The most used methods for the evaluation of biofilms are referred to as either direct or indirect methods. Direct methods of quantifying biofilms use direct observation to quantify the desired parameters, such as colonies' count (CFU/mL) of sessile cells comprising biofilm structure (Adetunji and Odetokun, 2012; Asséré et al., 2008), visualization using specialized microscopes and staining with specific dyes (Marra et al., 2022; Wilson et al., 2017) that are selected according to the chemical properties of the dye and the specimen being stained, which determines the reaction between them. They provoke the destruction of the biofilm surface by scraping and homogenizing the biofilm for counting the number of cells and by applying a pigment layer onto the biofilm surface during the staining, either for imaging or for counting cells. Besides, bacteria enumeration is straightforwardly associated with biofilm, only at the early stages of formation, since at later stages of biofilm growth EPS contributes as well, masking the impact of live cells (Nakagawa et al., 2022). Also, visualizing and staining procedures, even though they can provide convenient and qualitative evaluation, need specialized and expensive equipment and consumables and are not appropriate for monitoring in-situ. Biofilm growth can also be characterized indirectly using dry mass determination, total organic carbon, crystal violet staining and total protein determination (Wilson et al., 2017). Although these methods are easy and inexpensive to perform, they lead, nevertheless, to the destruction of the samples with difficulties related to the viability and separation of cell mass from other existing components comprising the biofilm. Moreover, results present significant uncertainties and refer to a single point measurement at a specific time.

The structure of biofilms is usually evaluated using microscopy analysis based on Atomic Force Microscopy (AFM) (Chatterjee et al., 2014), Confocal Laser Scanning Microscopy (CLSM) (Schlafer and Meyer, 2017), Transmission Electron Microscopy (TEM) and Scanning Electron Microscopy (SEM) (McCutcheon and Southam, 2018). However, such techniques are quite costly and require sophisticated microscopy and material preparation tools to implement them. Although real-time monitoring of the biofilm structure can be achieved using CLSM under controlled conditions in specific systems, the rest of the techniques require destruction of the samples.

Non-destructive techniques for biofilm monitoring have been developed aiming to overcome the above limitations. Chen et al. (2010) used Quartz Crystal Microbalance (QCM), a non-destructive process to detect early formation of biofilms. Likewise, Olsson et al. (2015) used the same technique to detect the initial adhesion of organisms, however, the biofilm was detected only on the surface provided by QCM; as such, this technique cannot be employed in a wide range of applications. Thermal Lens Microscopy (TLM), another application for monitoring biofilm was used in microchannels and flow cells (Roβteuscher, 2009), measuring the photothermal effect inside the sample. This method is rather promising due to its ability to detect biofilms, while it offers staining-free observation of biofilms despite its limitations in the observation area, detection limit and resolution.

Electrochemical Impedance Spectroscopy (EIS) has also been used to assess cell growth and biofilm development demonstrating several advantages of high sensitivity, selectivity, and fast response. EIS based sensors for detecting biofilm formation have been employed in a wide range of systems, like Petri dishes, modified CDC reactors that simulate the conditions in vivo (Bruchmann et al., 2015) and most commonly in well microtiter plates (Chabowski et al., 2015; Guła et al., 2020; Paredes et al., 2013). Several studies focus on employing EIS for the detection and changes of free-floating cells, while others on the evaluation of biofilm development and some of both phenomena. For example, Giaever and Keese (1993) used EIS to characterize the changes in morphology of adherent cells from different cultures. Kim et al. (2011), in addition, with an improved electrochemical monitoring system achieved the evaluation of biofilm development, due to removal of planktonic bacteria by introducing fresh electrolyte inside the experimental system. Furthermore, other studies performed by Paredes et al. (2012) and Guła et al. (2020) showed the ability of EIS for measuring both cell changes inside the investigated system and also changes due to biofilm development and growth. In such studies, the decrease of impedance is attributed to the increase in number of cells (Bayoudh et al., 2008), while on the contrary, in other studies cell growth causes the increase of impedance (Gamal et al., 2018). Additionally, in some investigations the increase of impedance is associated with the increase of surface coverage with biofilm (Bruchmann et al., 2015; Song et al., 2020), while Turolla et al. (2019) supported that biofilm increase development leads to impedance, due to the prevalence of the extracellular matrix conductivity.

In these cases, the detection of cell growth and/or biofilm development is based on the interactions between cells and other constituents, like EPS, salts, nutrients, gas bubbles and the surface of the electrode that is normally introduced to the test system. These phenomena alter the impedance and/or capacitance of the test system (Gkotsis et al., 2020; Oikonomidou et al., 2018). The idea of this study is to use the substrate surface, where the biofilm is developed, as the electrode of EIS technique.

It should be stressed though that in all above applications, the biofilm is detected through its development on the interface between the electrode surface and the bulk medium. However, in these cases the obtained results cannot be projected to the surface of interest, e.g. the material of a water pipe. Therefore, mechanisms and interactions between electrode surface and bulk medium cannot be extrapolated to the system under investigation. Another limiting factor for the broad application of such electrodes is the material they are made of, which is mainly gold (Bruchmann et al., 2015), used to obtain high sensitivity and limit corrosion implications. In addition, the sensor placement implies the intervention in the system under investigation, while after the saturation of the electrode, the latter should be removed and cleaned or replaced.

Summarizing, while existing biofilm monitoring methods provide valuable information regarding biofilm structure, morphology, quantification, and other critical parameters, they do come with a set of inherent limitations, especially when biofilms are formed inside pipes or other flow cells. Such limitations include the need for disassembling the experimental setup, the sample destruction, high costs and inability to provide results in real time without interventions in the bulk flow. To confront these challenges, a system that is installed at the external part of a flow cell, able to record the biofilm changes inside this flow cell, should be developed.

To this aim, the objective of this study was to develop a sensitive, non-invasive electrical resistance spectroscopy technique that enables in real time detection of biofilms during the early stages of their formation and monitoring of their evolution, as well. Furthermore, this technique should be applied in real systems, to reveal the interactions between the substrate surface and the bulk medium; this requires the use of the wetted surfaces as electrodes that sense the modified voltage when biofilm grows. Unlike existing methods, which are often destructive or malfunctioning for real-world applications, our approach enables the early detection and continuous monitoring of biofilm formation. Using this novel approach, this study targets the direct sensing of biofilm

development on metallic surfaces of interest and not indirectly by sensing biofilm growth on the surface of an instrumental electrode (that is normally different from that of the biofilm substrate). In other words, in our technique the sensing electrode is the biofilm substrate itself. This unique method is a first step towards the future development of biofilm monitoring techniques, non-invasive, online, in real-world applications, such as water systems.

To this end, we investigated a modified type of electrical impedance method based on In-Vivo Embolic Detector (I-VED) hardware, patented by Karapantsios et al. (2016). This method is based on ultra-sensitive Alternating Current (AC) electrical impedance spectroscopy, developed for the detection of Coronary Artery Disease (Karapantsios et al., 2017; Tzevelecos et al., 2021). The electrical impedance of the bulk medium differs according to the constituents' concentrations, temperature, excitation frequency and liquid volume crossed by the AC excitation current. These factors are considered when validating this technique and extracting reliable results on biofilm development.

The proof of technology is implemented by developing and analyzing biofilms formed on metallic surfaces inside continuous flow water systems. For this purpose, single strain biofilms of *Pseudomonas fluorescens* are developed in a laboratory-scale test setup under static and laminar flow conditions at constant temperature. Throughout the duration of each experiment, the metallic surfaces are used as specific sensors that are properly mounted onto the flow setup, thus recording impedance changes during cell attachment and biofilm formation and growth. The impedance results are explained and validated using the morphological and topographical characterization of biofilm coated surfaces.

2. Materials and methods

2.1. Bacterial strain and culture conditions

Pseudomonas fluorescens AR 11 bacteria, Gram-negative, rod-shaped, mesophilic human pathogens that were isolated from raw milk for cheese production are provided by DSZM-German Collection of Microorganisms and Cell Cultures GmbH (Braunschweig, Germany). These bacteria can exhibit motility via motile polar flagella (Scales et al., 2014), their size is approximately 0.5 μm in width and ranges 2.0–2.5 μm in length (Martínez-García et al., 2015) and also possess a number of functional traits that provide the bacteria with the ability to form biofilms (Scales et al., 2014).

Bacterial cells are cultivated as explicitly described in Kampouraki et al., (2022).

2.2. Experimental set-up

2.2.1. Biofilm formation in flow cell

Biofilms are developed on passivated and electropolished stainless steel coupons SS316L (EP SS316L) used in previous studies (Kampouraki et al., 2022; Petala et al., 2017) under well-controlled conditions inside a flow cell. Temperature is kept constant at 27 °C ± 0.1 °C inside a climatic chamber, while tests are conducted either under static conditions or laminar flow conditions of the mineral medium. The cell consists of a base compartment, that carries a receptacle (Fig. 1 (2)) for placing two coupons (Fig. 1 (4)) along specific dimensions (length × width × depth: 76 × 12.7 × 1.6 mm), while a spacer of 3 mm height is placed above the coupons determines the cross-sectional area of the flow (Fig. 1 (5)). At the top there is an identical base, on which two coupons are adjusted accordingly (Fig. 1 (6)). Two valves are assembled to the top unit at the inlet (Fig. 1 (7)) and outlet (Fig. 1 (8)) of the liquid flow. The flow cell system is kept free of air bubbles by placing the cell in vertical position and maintaining the up-flow direction of the medium. The mineral medium that contains all nutrients is introduced to the flow cell from a flask via a peristaltic pump. The waste at the outlet of the flow cell is collected in a waste container. This setup allows continuous supply of nutrients and continuous flow of medium through the system.

Before each test, EP SS316L coupons are cleaned as described in the following procedure: cleaning with a commercial anionic surfactant, rinsing with tap water, immersion in 95% ethanol solution, rinsing with distilled water, and then drying at 50 °C overnight. The rest of the experimental set-up is sterilized with hydrogen peroxide solution (30% w/v) and rinsed with sterilized bi-distilled water. Each experiment starts with the assembling of the flow cell and the connections with peristaltic pump and flask containing the medium using tubes. Afterwards, the whole set up is sterilized again with hydrogen peroxide solution and sterilized with bi-distilled water before fresh and sterilized mineral medium enters through the flow cell for the final step of cleaning. All the components of the set-up including flow cell compartments, mineral medium and bacterial suspension after sterilization are kept inside the climate chamber overnight before the beginning of each experiment, to reach stable conditions before starting the electrical measurements. Subsequently, 10 mL of clean and sterilized mineral medium or 10 mL of

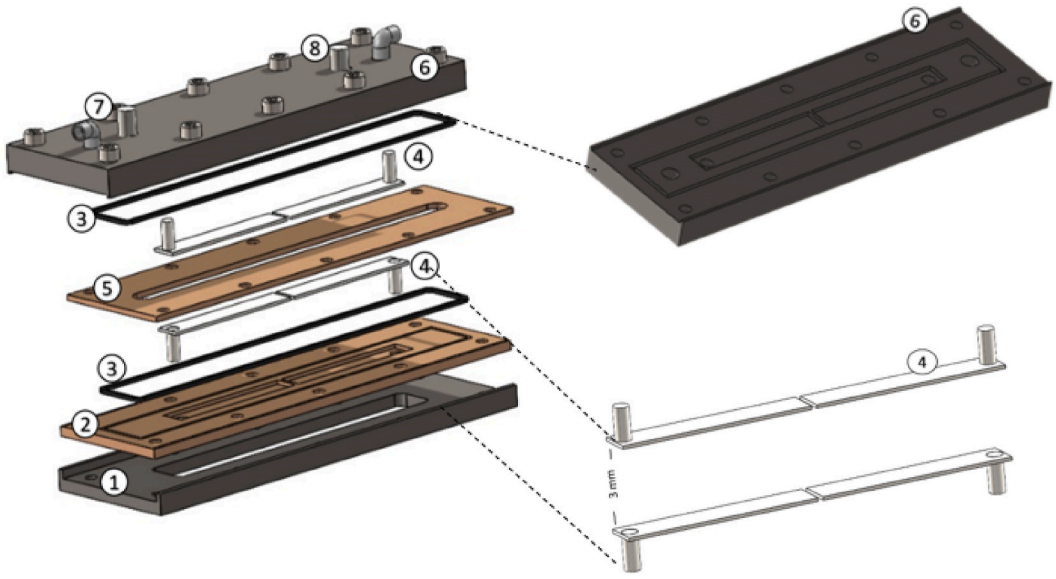

Fig. 1. 3D configuration of the flow cell components. Flow cells include: 1-Lower plate, 2-Coupon base, 3-O-Rings, 4-EP SS316L coupons connected with terminal leads, 5-Flow spacer, 6- details of top compartment, 7-nutrient medium input port, 8-electrode tip.

bacterial suspension of optical density equal to 0.5 cm^{-1}, are injected through the septum at the entrance valve of the flow cell. Following the above procedure, different and independent experiments are conducted with respect to liquid flow. Firstly, experiments under stagnant conditions are performed, on which the channel of the flow cell is either filled with mineral medium to test the effect of the liquid medium on resistance measurements or filled with bacterial suspension to evaluate the influence of bacteria to the recorded data.

Thereafter, another group of experiments is conducted to test the behavior of the system with continuous medium flow. For this reason, after the performance of cleaning procedure as described above, the cell is filled with mineral medium or bacterial suspension and is kept under stagnant conditions. Right after 2 h, a constant volumetric flow rate of 1.5 mL/min is applied for 24, 48 or 72 h, depending on the experiment and the parameters to be tested. All these tests run in triplicate and are repeated twice. Such experiments can simulate the flow and biofilm formation inside the pipes of a water system in laminar flow with Reynolds number equal to 3.38 according to the following equation:

$$Re = \frac{\rho\, v\, D_h}{\eta} \quad (1)$$

where ρ is the density of the fluid (kg m^{-3}), v is the flow velocity (m s^{-1}), η is the dynamic viscosity of the fluid (Pa s) and D_h is the hydraulic diameter. Since the flow cell is rectangular rather than circular in cross section, the hydraulic diameter is calculated by $D_h = 4A/c$, where A is the cross-sectional area and c is the wetted perimeter (Munson et al., 1990).

2.2.2. Electrical measurements

Electrical Impedance Spectroscopy (EIS), a non-invasive technique (modified I-VED® patented by Karapantsios and co-workers (Karapantsios et al., 2016), is modified and used in this study to monitor the evolution of biofilm formation on metallic surfaces (Evgenidis and Karapantsios, 2015, 2022). The growth of biofilm is monitored with continuous recording of electrical signals. This technique is based on the measurement of the real (resistive) component of the electrical impedance (complex number) of the system (including that of mineral medium) and its operating principle is based on the determination of the resistance increase, or equivalently the reduction of the electrical conductivity, that corresponds to the build-up of biofilm on the coupons' surface.

The experimental set-up includes, as shown in Fig. 2A, a signal generator (SG) with two independent output channels, that generates a sinusoidal voltage excitation of 1 Vp-p at 25 kHz for each channel, two 24 bit/192 kHz data acquisition cards Focusrite Scarlett 2i2 3rd Generation (DA), two terminal adjustable resistance boxes (RB) for signal tuning and two computers connected to the data acquisition cards used for real time monitoring and recording of the signals. The PVC flow cell that is used in this study includes metal terminal leads, on the top and the bottom of the cell, connected with the metallic coupons. All coupons act as electrodes in electrical contact with the medium (i.e., mineral medium or bacterial suspension) in the flow cell. These terminal leads are placed in pairs, two onto the first coupon set from the entrance of the flow cell (Fig. 2A(E_1, E_2)) and two onto the second (Fig. 2A(E_1', E_2')). The spacing between the two opposing coupons is 3 mm (as shown in Fig. 1), while the distance between two terminals in each pair is 68.65 mm.

The operation principle for this technique is based on calculating the ratio of the output voltage of the coupon to the input voltage from the signal generator. The input voltage (excitation) for each coupon pair is connected to the input terminal and is supplied by the corresponding independent output channel of the SG. That excitation induces an AC current that passes through the liquid between the electrodes/coupons that are assembled on the test flow cell and generates a voltage difference between input and output terminals due to the electrical resistance of the liquid (Ohm's law). As a result, due to Kirchhoff's second law the output voltage that is measured across the termination resistor depends on the electrical resistance between the coupons. The output and input voltages are acquired and recorded by a Data Acquisition Card, one for each coupon pair.

Although the I-VED's technique can provide resistance time series with sampling frequency of several thousand samples per second at a resolution better than 0.01%, the sampling frequency has been set to 200 Hz, since for the present application and the aim of the experiment this frequency adequately samples all frequency components of the measured signals.

Electrical signals are recorded every 60 min for 72 h. Each recording lasts for 30 s and the data are then transformed into resistance time series of high sampling frequency and resolution by the corresponding

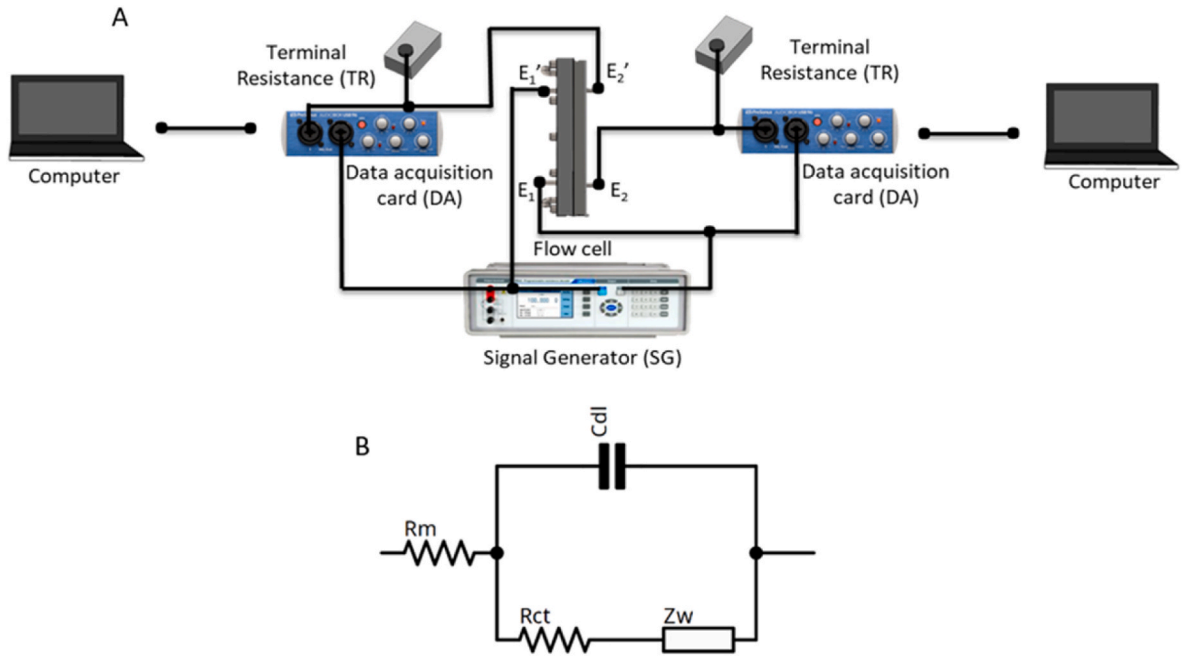

Fig. 2. A) Experimental setup of electrical measurements, B) Series equivalent electrical circuit of electrode/medium system.

algorithm. With proper calibration and constant temperature throughout the duration of the experiment, the measured voltages are directly related to the mineral medium electrical resistance and, therefore, to the biofilm surface and planktonic bacteria cells.

The impedance Z of electrode/medium system, when the coupon surface is in contact with the mineral medium, can be modeled with a Randles and Ershler electrical equivalent circuit (Furst and Francis, 2019; Magar et al., 2021). The model contains the resistance of the mineral medium R_m connected in series with the contact impedance Z_c of the electrode/medium interface, i.e. $Z = R_m + Z_c$. The contact impedance Z_c can be further analyzed as the parallel connection of the double layer capacitance C_{dl} component at the surface of the coupon with the series connection of the charge transfer resistance R_{ct} with the Warburg impedance Z_w. According to electrical circuits' theory, the contact impedance Z_c is given by Equation (2):

$$\frac{1}{Z_c} = \frac{1}{X_{Cdl}} + \frac{1}{R_{ct} + Z_w} \tag{2}$$

The corresponding equivalent electrical circuit is shown in Fig. 2B.

The impedance Z of the electrode/medium system is given by Equation (3):

$$Z = R_m + Z_c = R_m + X_{Cdl}\frac{R_{ct} + Z_w}{X_{Cdl} + R_{ct} + Z_w} \tag{3}$$

where $X_{Cdl} = {}^{1}/_{j\omega C_{dl}}$ is the reactance of the double layer capacitance. Typical values of C_{dl} are 10–40 μF/cm^2 and depend on the ion concentration as well as the material of the electrodes (Tzevelecos et al., 2021). Considering the 9.65 cm^2 surface of the electrode, the total double layer capacitance would be 96.5–386 μF. At high excitation frequencies greater than 10 kHz, the reactance of the double layer capacitance would be very low, effectively "short circuit" and minimizing the influence of both R_{ct} and Z_w on Z. Even for the minimum value of double layer capacitance C_{dl}, the maximum value of X_{Cdl} is 0.2 Ω. For all experiments the conductivity of the mineral solution was such so the resistance R_m is in order of 10 Ω, at least 10 times greater that X_{Cdl}, leading to a negligible effect of contact impedance. In addition, due to the parallel connection of C_{dl} with the series connection of R_{ct} and Z_w, the contact impedance Z_c would be less than the value of X_{Cdl} alone.

According to the theory of electrical systems, the voltage transfer function H(jω) of an electrical circuit is the ratio of the output voltage V_o to the input voltage V_i, defined in the following equation:

$$H(j\omega) = \frac{V_o e^{i\omega t+\varphi 1}}{V_i e^{i\omega t+\varphi 2}} = \frac{V_o}{V_i} e^{i\omega t+\Delta\varphi} \tag{4}$$

The phase difference $\Delta\varphi$ indicates the resistive or not response of the circuit. If $\Delta\varphi = 0^\circ$ then the circuit contains only resistors and therefore resistive response. If $\Delta\varphi \neq 0^\circ$, then the circuit contains reactive components as well. Negative $\Delta\varphi$ values indicate capacitive response and positive values inductive response. For the extreme cases of $\Delta\varphi = \pm 90^\circ$ the circuit is composed of Constant Phase Element (CPE) (Moradi et al., 2022), i.e. ideal reactive components. If $\Delta\varphi = +90^\circ$, then the circuit is an ideal inductor, whilst $\Delta\varphi = -90^\circ$ the circuit is an ideal capacitor. The value of phase difference Δφ is frequency dependent for the non-resistive case.

With the intention of finding the optimum excitation frequency where the influence of reactive components on Z is minimized, experiments were conducted with frequency scanning from 10 to 85 kHz, as shown in Fig. 3A. The phase difference $\Delta\varphi$ was measured between the output and input voltages of the two pairs of electrodes of the system, whilst the liquid medium was present. From Fig. 3A, it is shown that for the two pairs of electrodes the phase difference is negligible for the full scanned frequency range, indicating resistive response of the liquid medium and the flow cell. The phase difference is minimized in the frequency from 20 kHz to 30 kHz for both pairs of coupons; therefore, the excitation frequency of the SG was set to 25 kHz. At 25 kHz the phase difference is $\Delta\varphi = 1.5^\circ$ and the ratio of imaginary part to the real part is $X_{/R} = tan(\Delta\varphi) = 0.03$.

At such frequencies the phase difference is minimized, hence the imaginary part of equation (2) is negligible. The response is dominated by the real part and the impedance Z of the electrode/medium is simplified to the resistance of the mineral medium $Z = R_m$. The lipopolysaccharide cell membrane of the bacteria is insulating due to the presence of inherent permeability barrier capacity, so when attached to the coupon surface, the insulating properties reduce the surface that is in contact with mineral medium leading to an increase of the flow cell resistance (Furst and Francis, 2019). Therefore, when the flow cell is filled with bacterial suspension, the composition resistance is the mineral medium resistance increased by the resistance of the biofilm. The corresponding representative electrical equivalent circuit of the test flow for the one pair of electrodes of Fig. 2 is presented in Fig. 3B.

As it is shown in Fig. 3B, the resistors R_m and R_t are connected in series and constitute a voltage divider. Therefore, the voltage ratio k of the output (V_0) voltage over the input voltage (V_i) is given by:

$$k = \frac{V_0}{V_i} = \frac{R_t}{R_m + R_t} \tag{5}$$

where R_t is the terminal resistance of the decay box, that is set in the beginning of the experiment by the operator and R_m is the resistance between the pair of electrodes on the flow cell, that depends on the mineral medium composition. Rearranging Eq. (5) the resistance of the

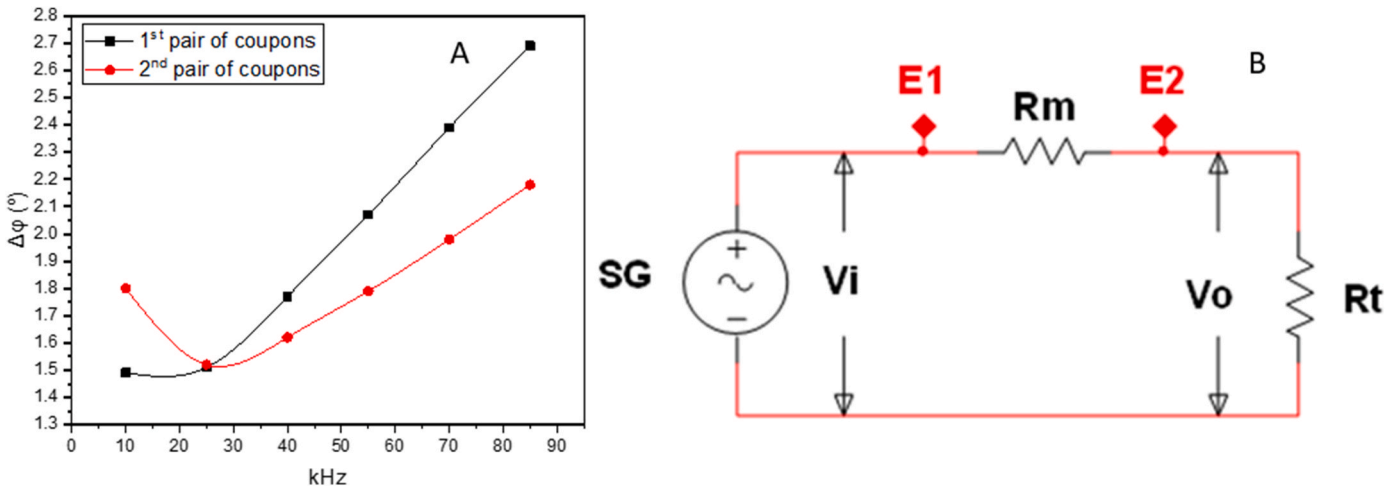

Fig. 3. A) Phase difference Δφ between the output and input voltages of the two pairs of electrodes of the system, B) Electrical equivalent circuit of the test flow.

mineral medium can be calculated as:

$$R_m = \left(k^{-1} - 1\right)R_t \quad (6)$$

In each experiment the recorded signals V_0 and V_i are used for the calculation of resistance time series and are given in terms of normalized resistance values derived from the ratio of average resistance per hour to the recorded initial resistance value.

2.3. Characterization of biofilm surface and bulk liquid

Morphological parameters of biofilm coated surfaces are determined by microscopy examination at different spots of the same coupon and on different coupons of the same experiment, to ensure the repeatability and the reliability of the measurements. Three-dimensional surface topography of different coupons is evaluated with 3D Optical Surface Metrology System Leica DCM8 device, after their dehydration, at ambient conditions. The same spots at the same coupons were selected at different experiment days' coupons using 20× magnification lens, depicting an area 850 × 650 μm, for the determination of the roughness profile (Sdr, %), the 3D view of the surface, the maximum height of the surface (Sz, μm) and the root mean square height of the surface (Sq, μm), parameters that can characterize the thickness of the surface. The topography layer is described with parameters that involve only the statistical distribution of height values along the z-axis, according to ISO 25178 (International Organization for Standardization, 2012). Biofilm images, captured by Leica DCM8 microscope, are processed with the commercial software Image Pro Plus 6.0 (Media Cybernetics, Inc) to define the biofilm coverage area percentage over the total area. Each image is analyzed by calculating the area of the developed biofilm.

Additionally, biofilm-coated surfaces are also subjected to imaging, using Optical Coherence Tomography (OCT) (Ganymede, Thorlabs) at 24, 48 and 72 h of the cultivation with the objective lens OCT-LK3. OCT possesses the capability to both scan for and discern biofilm thickness, as well as perform a tomographic evaluation of the biofilm structure. This is made possible by the acquisition of high-resolution images in a non-invasive manner, without causing any harm to the sample. The spatial resolution of acquired OCT images is not fixed, as it depends on a number of operational parameters, but in all cases is less than 1μm/pixel. Following the scanning process at various locations across the entire metallic surface, two-dimensional images are obtained. High resolution biofilm images were processed by a custom-made configurable Matlab software. Substrate and biofilm contour points are automatically detected in order to calculate biofilm thickness for every point in x-axis. Bottom right legend is processed automatically in order to convert pixel metrics to world metrics (mm). The above calculations are based on the following methods: two dimensions median filtering, intensity thresholding, connected components computation and exterior and internal holes boundaries tracing.

To assess the bacterial population adhered to individual EP SS316L coupons, scratching of each coupon is performed with a sterile toothbrush, which is then immersed in 5 mL of a sterile phosphate solution. Afterwards, the turbidity of the re-suspended biofilm is measured at 600 nm (OD600nm). Besides that, the dry mass of each biofilm is determined by drying the biofilm coated substrate at 40 °C overnight, measuring the weight and subtracting the substrate net weight.

During each experiment the quality of bulk liquid is also characterized in terms of dissolved oxygen consumption and optical density. Dissolved oxygen is determined by measuring the oxygen (HQ 30D, Hach) in the medium at the inlet and the outlet of the flow cell. In parallel, the turbidity of the samples at 600 nm (OD_{600nm}) is measured (UV-1800 SHIMADZU Spectrophotometer) to evaluate the concentration of biomass. The evolution of glucose concentration within bacterial suspensions is also estimated according to the sulfuric acid-phenol protocol, previously described by Castigliano et al. (2021) for the bulk liquid at 24, 48 and 72 h of incubation time. Furthermore, the Dissolved Organic Carbon (DOC) of the bulk is also analyzed aiming to quantify the organic matter remaining in the liquid.

3. Results and discussion

To examine whether electrical resistance technique can be used as a tool for direct measurement of biofilm growth in closed water systems, an extensive and methodological approach has been adopted. Initially, the electrical technique setup was established realizing the critical parameters for accurate measurements. Afterwards, this novel sensing system is applied to two different modes of biofilm growth: static and under constant water flow. Electrical signals are then compared and qualitatively related to microscopic observations. Novel characteristics of this method rely on the setup configuration that enables flexible adjustment to other metallic water systems, elimination of electrical signal misinterpretations due to bulk water characteristics and direct evaluation of biofilm growth rates.

Pseudomonas fluorescens biofilms are developed under static or laminar flow conditions inside test cells at constant temperature of 27 °C ± 0.1 °C onto EP SS316L coupons. The resistance of the system is measured throughout the experiment duration, while after 24, 48 and 72 h, the coupons are removed to characterize the morphology and topography of the obtained biofilms by optical means using 3D metrology microscope. In parallel, the liquid collected at the outlet of the flow cell is submitted to turbidity (OD600 nm) measurements for evaluation of the presence of planktonic bacteria, and to dissolved oxygen concentration measurements to assess the oxygen consumption inside the test cell.

3.1. Electrical measurements

In contrast to most impedance spectroscopy studies that measure biofilms at distinct points in biofilm maturation time, in our study it is explored whether continuous measurements can in fact capture the dynamics of biofilm formation. To avoid misleading results, initial experiments are conducted to evaluate the critical parameters of the experimental setup that influence the output signals of the electrical resistance technique. First, tests were conducted to verify the stability and sensitivity of the electrical system in terms of measuring resistance. Subsequently, the effect of the mineral medium inside the flow cell is investigated before and after the injection of bacteria suspension. Then, the impact of the flow on the electrical measurements is examined, as well as the effect of liquid suspension of bacteria on these measurements. The results of these tests verified that changes in electrical signal correspond to alterations in biofilm development.

3.1.1. Electrical signal

When measuring impedance or resistance in complex multiphase systems, it is essential to test the stability and the response of the electrical system focusing on the electrical signals without the presence of a liquid solution. For this reason, the flow cell can be simulated with the electrical equivalent of two 10 Ω resistors, one for each pair of electrode/coupons.

Fig. 4A shows that the measured resistance value remains stable and almost identical for both pairs of coupons, confirming the stability of the recorded signals and electrical system after 72 h of the experiment duration. In addition, as it is shown in Fig. 4B, the Coefficient of Variation (CV, the ratio of standard deviation to mean resistance) is in the order of 10^{-4} or 80 dB Signal-to-Noise ratio (SNR), verifying the high sensitivity of the electrical system and capability to measure miniscule resistance variations. Mean resistance values are shown in Fig. S1, as well. Moreover, the stability and the high SNR of the signal implies that when bacteria are inside the flow cell along with mineral medium, the observed changes in the signal will correspond to the changes inside the flow cell, e.g. changes in planktonic bacteria concentration, surface coverage by biofilm, etc.

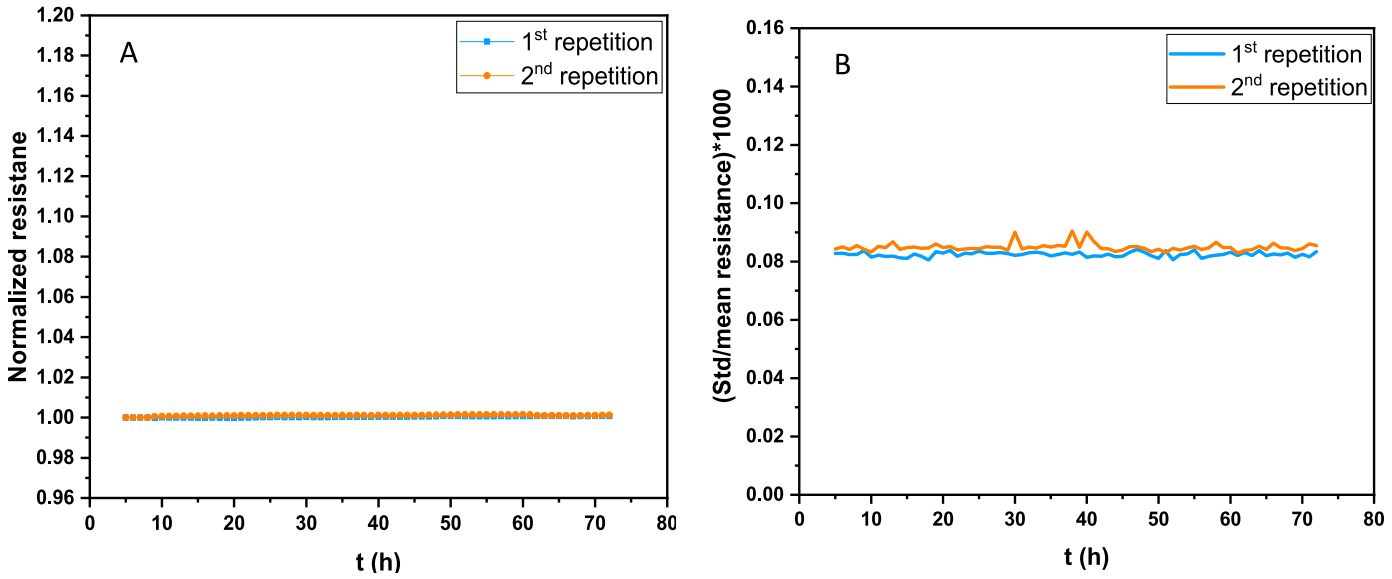

Fig. 4. Experimental test of electrical signal: A) Electrical measurements of normalized mean resistance with the time, B) Measurements of standard deviation to mean resistance with the time.

3.1.2. Measurements of mineral medium after the inoculation of bacteria

A crucial factor that can possibly affect the measurements is the presence of planktonic bacteria in the bulk water that swim inside the test cell. For this reason, three liquid bacterial suspensions of different initial concentration (different optical density) are prepared and are consequently introduced to the flow cell. As there is no biofilm formation yet on the system's coupons, the resistance measurements refer only to the liquid inside the cell. More specifically, each experiment starts with the initial measurement of the resistance of mineral medium and continues afterwards with each bacteria suspension. From the results, shown in Fig. 5, it can be seen that the resistance remains almost stable, confirming that planktonic bacteria do not affect the resistance of the system. The latter was rather expected, since free-swimming bacteria do not significantly alter the conductivity of bulk medium, as concluded from conductivity measurements of mineral medium enriched with bacteria cultures (data not shown).

3.1.3. Experiments without mineral medium flow (stagnant conditions)

The impact of liquid mineral medium and the effect of bacterial suspension inside the flow cell are further investigated with respect to electrical signal. To this aim, mineral medium is introduced to the test cell and is left at stagnant conditions for 72 h. Fig. 6 clearly demonstrates that the resistance remains stable with negligible deviations from the average values. Thus, the mineral medium by itself does not affect the electrical measurements. On the contrary, an increase of the normalized electrical resistance is recorded after the injection of bacterial suspension. The resistance increases sharply up to about 15 h of bacterial retention inside the flow cell, while afterwards the electrical signal remains rather stable. The normalized resistance is around 5.5% higher compared to that of medium without bacteria and is attributed to the attachment of bacteria on the metallic surfaces. The subsequent stabilization of the signal implies suppression of the microbial activities. Indeed, dissolved oxygen and glucose are completely consumed after 24 h of the experiment, while the optical density of the medium inside the

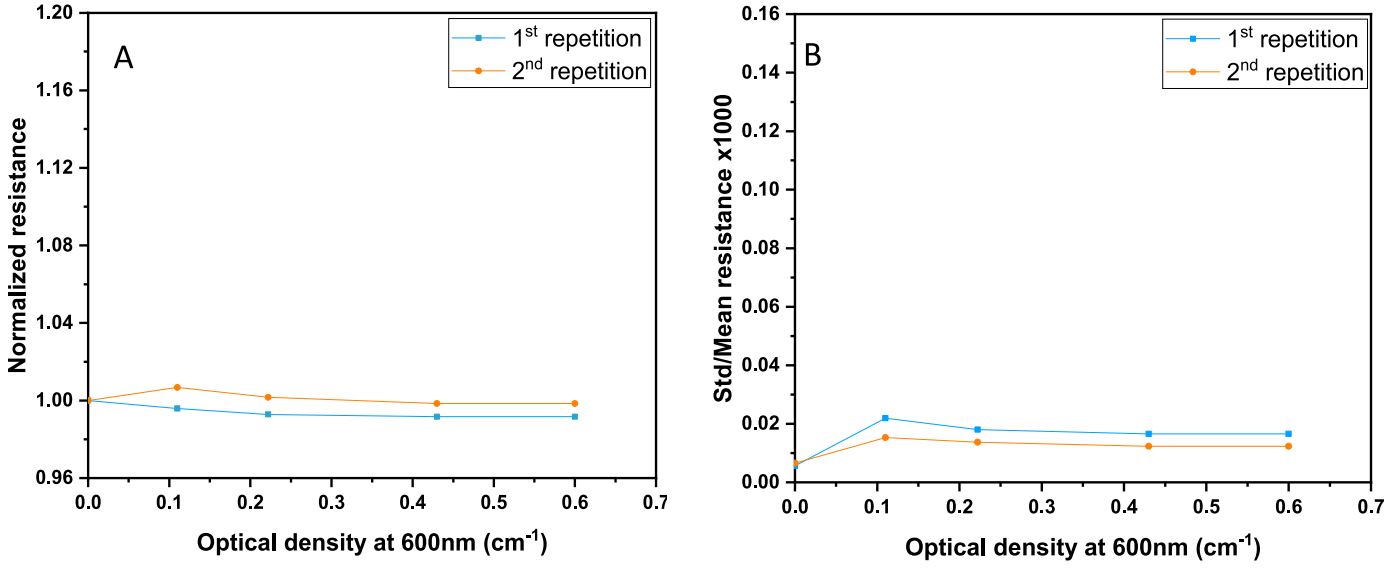

Fig. 5. Electrical measurements with different optical density of bacteria suspensions: A) Normalized mean resistance of medium with different bacteria suspension densities, B) Standard deviation to mean resistance of medium with different bacteria suspension densities.

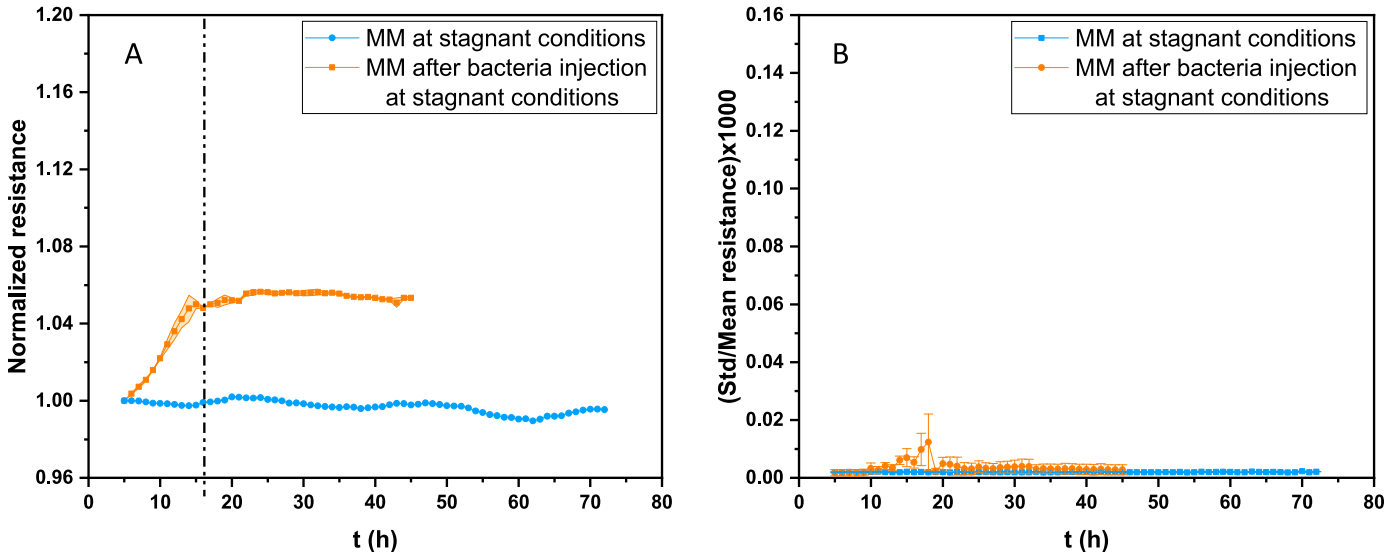

Fig. 6. Electrical measurements of mineral medium and mineral medium after the injection of bacteria at stagnant conditions and constant temperature. A) Normalized mean resistances vs. time, B) Standard deviation to mean resistance vs. time. Additional similar experiments are shown in Fig. S2.

test cell drops from 0.5 cm^{-1} at the beginning of the experiment to below 0.1 cm^{-1} at the end. Under such conditions the development of biofilm is hindered. Moreover, after 48 h of retention time, bubbles are formed inside the cell that increase considerably the resistance of the system, thus masking the output signals that refer to biofilm maturation. This is why the normalized resistance is shown up to 48 h in Fig. 6. The results of Fig. 6 confirm once more that planktonic bacteria do not significantly contribute to the output signal, since the signal is stable whereas in the meantime the planktonic bacteria are reduced. The maximum optical density of the bulk medium did not exceed 0.6 cm^{-1}, the maximum tested value (Fig. 5).

The morphology and topography of biofilms formed after 6 and 10 h of the experiment are demonstrated in Figs. 7 and 8, to realize the phenomena occurring during various stages of normalized resistance increase (Fig. 6A). Experiments are performed in triplicate and the results confirm the resistance measurements. It is noticed that after 6 h and 10 h of incubation the biofilm formation remains at the very early stages. Comparing images of clean EP SS316L surfaces (Fig. 7A) with corresponding images after 6 h (Fig. 7B) and 10 h (Fig. 7C) of incubation, the adhesion of bacteria and the formation of more complex structures that imply biofilms presence over the examined surface are noticed. The biofilm structures are augmented with incubation time, along with the surface coverage area.

To confirm the microscopic observations, image analysis is performed, to measure the increase of biofilm surface coverage area. Different spots of the same coupons and spots from different experiments are tested, verifying that coverage of the surface is increased. Particularly, after 6 h of biofilm formation the coverage area is calculated to be 8.3 ± 1.9% and rises to 15.5 ± 2.9% right after 10 h. Likewise, from a topographical point of view, a gradual increase of roughness (Sdr, %) is observed with the increase of incubation time (Fig. 8). More particularly, a low value of surface roughness is measured on the clean sterile EP SS316L surface (Sdr = 0.050 ± 0.004%). After 6 h of biofilm formation a higher value is observed (Sdr = 0.071 ± 0.003%). This increase most probably appears due to the disperse adherence of cells on the metallic surface, as shown in microscopy images (Fig. 7B). Finally, further increase (Sdr = 0.105 ± 0.029%) is perceived after 10 h of incubation, that goes along with the microscopy images (Fig. 7C), in which a higher number of adherent cells is observed within larger and denser structures of biofilm clusters.

3.1.4. *Continuous-flow experiments*

During continuous flow experiments, the flow rate of mineral medium equals to 1.5 mL/min. Two types of experiments are performed: a control test, during which only mineral medium passes through the test cell, and an actual test, during which medium passes through the test cell after bacterial inoculation. Single mineral medium passage through the test cell does not induce alterations in the electrical signal output. Normalized relative resistance values are rather stable (Fig. 9B) demonstrating low standard deviations among repetitions. In the case of continuous flow of medium after inoculation with bacteria, a continuous increase of the resistance is observed (Fig. 9). All repetitions show comparable behavior up to 72 h of experiment. More specifically, there is a slight slope during the first hours of the experiments, that is probably attributed to the initial lag phase of cells proliferation, in which the cells are spread on all wetted surfaces of the test setup. After around 15 h, a sharp increase of the normalized resistance values is observed most probably due to the exponential phase of cells proliferation. Finally, after 48–50 h of the experiment, the rate of resistance increase declines, while the standard deviation is increased, as the slope of resistance increase among repetitions significantly differs. Comparing the in-flow experiments with mineral medium and the experiments after the inoculation with bacteria, the increase of normalized resistance is around 15%, which is a considerable difference taking into account the sensitivity and accuracy of the resistance measurements.

For further analysis of the experimental resistance results, the analysis of resistance time series is implemented. In Fig. S3A, the analysis of resistance time series with sampling frequency of 200 Hz in experiments without bacteria inoculation at specific signal data samplings is presented; whereas, in Fig. S3B, the results that correspond to experiments after bacteria inoculation are depicted. In all cases shown in Fig. S3A, resistance values are very close to the average values and the deviation values are clearly below 0.1%. Periodic peaks on the resistance time series (e.g. Fig. S3, t = 30 h) refer to the pumping step of the peristaltic pump. After the bacteria inoculation (Fig. S3B), the deviation for the average value increases, especially after 30 h of the experiment, but still not exceeding 0.2%.

By optical means, as proven by microscopy images (Fig. 10) at 24 h of the experiment there is an increase of biofilm surface area coverage to 49.6% ± 4.8%, while at 48 and 72 h of the experiment, the area coverage is increased to 99.9 and 100% correspondingly, i.e., full coverage of the metallic surface with biofilm (Table 1). Topographical characteristics are, thereafter, examined for a better understanding of

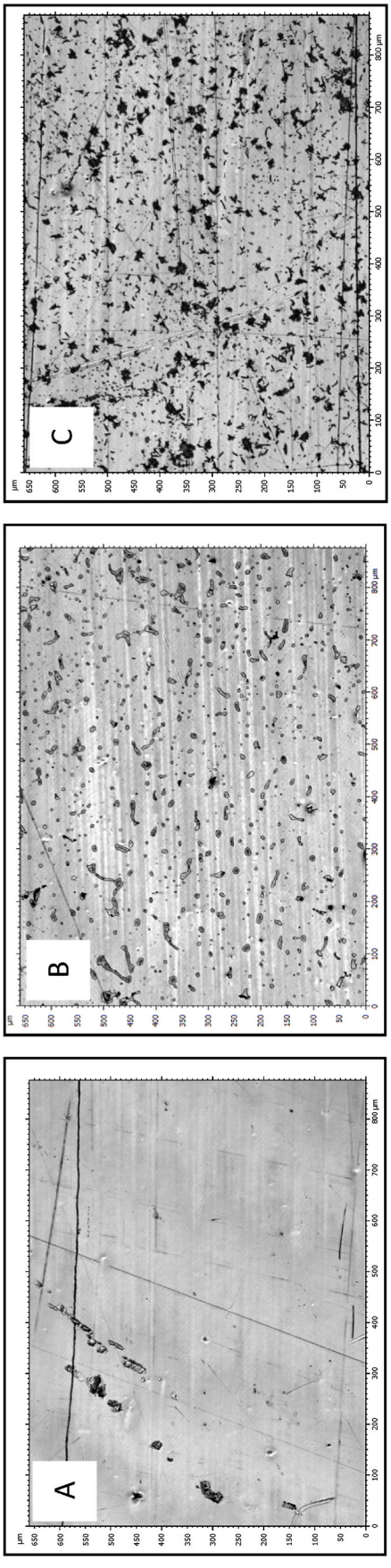

Fig. 7. Images of stainless steel electropolished (EP SS316L) coupons. (A) Clean EP SS316L surface. Biofilm-coated surfaces at different incubation periods of (B) 6 h and (C) 10 h, magnification 20×, area (850 × 650) μm^2.

the evolution and biofilm development on the surfaces with time. Profilometric 3D images (Fig. 11), captured from different spots of the coupons, confirm the results of optical images in accordance with the electrical measurements, as the increase of biofilm surface on EPSS 316 L coupons with the time and, in parallel, the increase of biofilm thickness onto the coupons at 48 and 72 h of the experiment, are visible. More specifically, as shown in Table 1, the Sz and Sq values continuously increase during 72 h of the experiment. The maximum height of the surface (Sz) starts from 1.50 μm (Fig. 11A) for the clean surface, due to the intrinsic roughness of the surface, increases slightly by 0.11 μm after 24 h, and further increases by 1.31 μm and 2.73 μm after 48 and 72 h, respectively, when compared to the clean surface (Table 1). Correspondingly, the root mean square height (Sq) starts from 0.25 μm (data not shown) for the clean surface, hardly increases by 0.01 μm after 24 h of the experiment and increases by 0.23 and 0.29 μm after 48 and 72 h of the experiment, respectively, when compared to the clean surface (Table 1). According to these results, as shown also in Fig. S4 the sharp increase of normalized resistance after 15 h and the declined rate of resistance increase after 48–50 h of the experiment is most probably due to the increase of biofilm surface coverage area, as the coverage seems to prevail the biofilm thickness on the electrical measurements of this system.

The roughness of the surface (Sdr, %), shown in Tables 1 and is compatible with the above observations, with a small value of roughness for the clean EP SS316L surface (Sdr = 0.038 ± 0.012%). With the increase of incubation time, the roughness increases to 0.061 ± 0.012% after 24 h, 0.094 ± 0.023% and 0.121 ± 0.055% after 48 and 72 h of the experiment, respectively. This is probably due to heterogenous increase of biofilm thickness, the study of which is rather challenging considering that the biofilm substratum already presents roughness. Consequently, biofilm thickness should be described using further analysis parameters.

A quantitative estimation of the biofilm growth is obtained after scratching of surfaces and subsequent determination of the optical density at 600 nm. Using this method, the measured optical density is 0.468 cm^{-1} after 24 h of incubation time, while after 48 and 72 h, twofold- (0.821 cm^{-1}) and threefold- (1.203 cm^{-1}) increase is observed, respectively (Fig. S5). Likewise, dry mass measurements reveal growth of biomass around 0.8 mg after 24 h of incubation, and 1.5 and 2.2 mg after 48 and 72 h, respectively (Fig. S5).

For the determination of the evolution of biofilm thickness and morphology, OCT measurements are performed at different incubation times (24, 48, 72 h). In Fig. 12, the 2D images of biofilm-coated surfaces are presented. After 24 h of test period, the images display a sparse distribution of microbial cells that form a thin biofilm layer (Fig. 12A). The mean biofilm thickness at this stage is observed to be around 29.9 ± 13.6 μm (Fig. 12A). This observation is confirmed also by the findings derived from surface topography analysis. However, as the test period is extended to 48 h, the biofilm thickness, is notably increased to approximately 50.3 ± 17.3 μm (Fig. 12B), with almost full coverage of the surface which is confirmed by the microscope observations. In this case, the biofilm is noticeably increased in thickness and displays a denser network of microbial cell. This increase after 48 h of the experiment suggests an ongoing and dynamic process of biofilm growth and maturation. Additionally, after 72 h, the biofilm thickness is further intensified, reaching approximately 148.5 ± 62.4 μm (Fig. 12C).

The images demonstrate not only the evolution of biofilm thickness in time, but also signify a progressive increase in biofilm biomass and structural complexity over the course of the experiment.

During the experimental period, an increase of planktonic bacteria population is observed along with elevated oxygen consumption, as shown in Fig. S6. Significant changes in glucose concentration and Dissolved Organic Carbon (DOC) levels are noticed over time. Initially, the glucose concentration is 1000 g/L but decreases to 231 g/L after 48 h, eventually reaching 0 g/L after 72 h of incubation. Similarly, the DOC content in the fresh medium starts at 480 g/L but exhibits a continuous decline over the test period. After 24 h, it decreases to 434 g/L, further

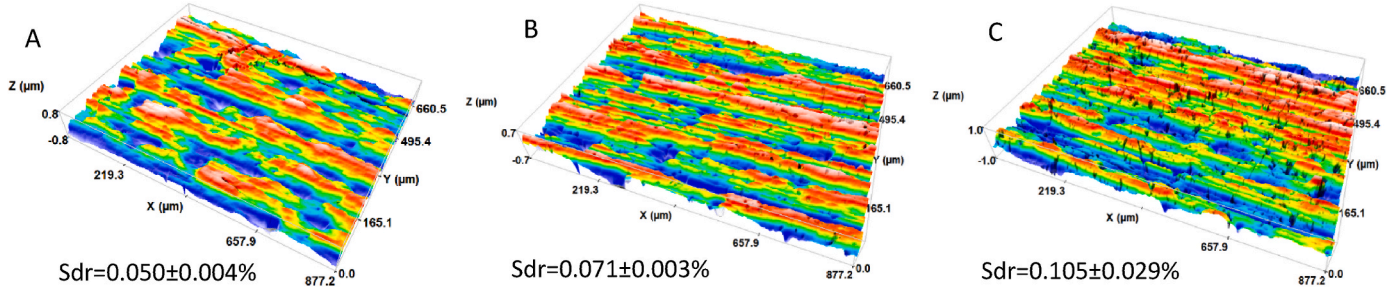

Fig. 8. Profilometric images of biofilms grown under static conditions at different incubation times (A) 0 h, (B) 6 h, (C) 10 h, magnification 20×, area (850 × 650) μm^2.

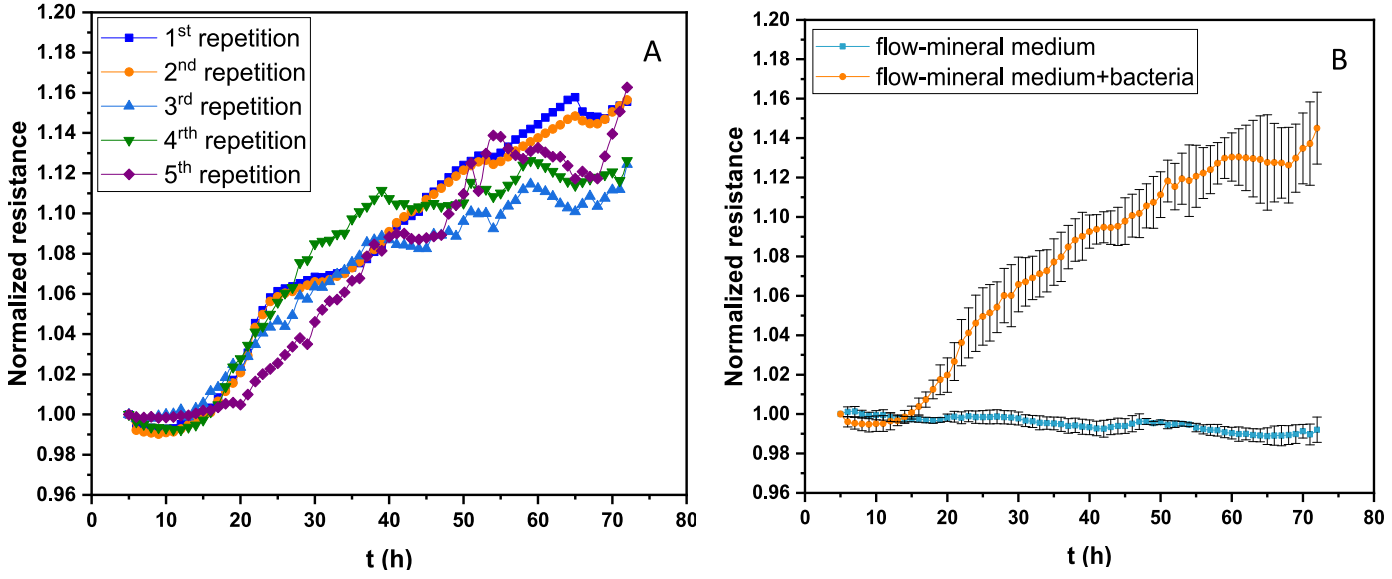

Fig. 9. Electrical measurements under laminar flow conditions (1.5 mL/min) at constant temperature in the presence and absence of bacteria for 72 h. A) Different repetitions of normalized resistance measurements values after the injection of bacteria and mineral medium flow, B) Mean normalized measured resistance values after single mineral medium flow through the test cell (blue lines) and after the injection of bacteria and mineral medium flow (orange lines).

reduces to 317 g/L at 48 h, and finally reaches 270 g/L after 72 h of the experiment. The observed changes in glucose concentration versus the DOC levels indicate the rapid consumption of glucose as food source, which is metabolized (also formation of EPS) but is not completely degraded.

Planktonic bacteria do not contribute to the increase of resistance and so does the mineral medium, while the response of electric components of the electrical circuit remain stable. Therefore, the increase of resistance is solely attributed to biofilm formation.

The results of this study confirm the capacity of this electrical resistant setup to capture biofilm growth on wetted metallic surfaces. By introducing such a non-invasive and real-time method for monitoring biofilms, better understanding of the dynamics of biofilms' development in various real-world applications can be achieved. Moreover, short- and/or long-term efficiency of antimicrobials/disinfectants can be estimated in situ. Alongside, contamination of the bulk medium due to the biofilm detachment can also be detected.

4. Conclusions

The development of an innovative non-invasive electrical resistance technique for monitoring biofilm formation and growth on metallic surfaces inside water flow systems is studied in this work. The developed technique uses the modified I-VED hardware and can provide high resolution data to detect the corresponding resistance changes during biofilm formation and growth. Electrical measurements are conducted through metallic electrodes/sensors that constitute part of the wall of the flow setup either under static or under flow conditions.

In parallel, the structural characteristics of biofilms formed on these metallic surfaces are examined by optical means. It is shown that electrical signals remain stable in all cases when no bacteria are present, while an increase is observed in experiments where bacteria are introduced to the flow channel. This increase is attributed to biofilm formation and growth on the metallic surfaces, which is higher in flow experiments than in static ones due to the continuous feed of bacteria with mineral medium. This hypothesis is confirmed by the morphological and topographical characteristics of the biofilm-coated surfaces, such as an increase in the biofilm coverage area, in biofilm surface roughness and in biofilm thickness.

This study provides evidence that the present electrical impedance technique is an efficient non-invasive real-time monitoring tool in flowing water systems, capable of monitoring biofilm growth on metallic surfaces. The non-destructive and non-invasive nature of the technique allows collecting online data of biofilm growth without interruption of the experiment to disassemble the experimental set up. In addition, the high sensitivity of electrical measurements offers the advantage that surface coverage and biofilm thickness can be registered simultaneously.

Cross examination of electrical signals with biofilm structural characteristics obtained by optical means, over a broad range of conditions will shed light on the underlying phenomena of biofilm growth and will allow better controlling of the biofilm formation in water systems, thus

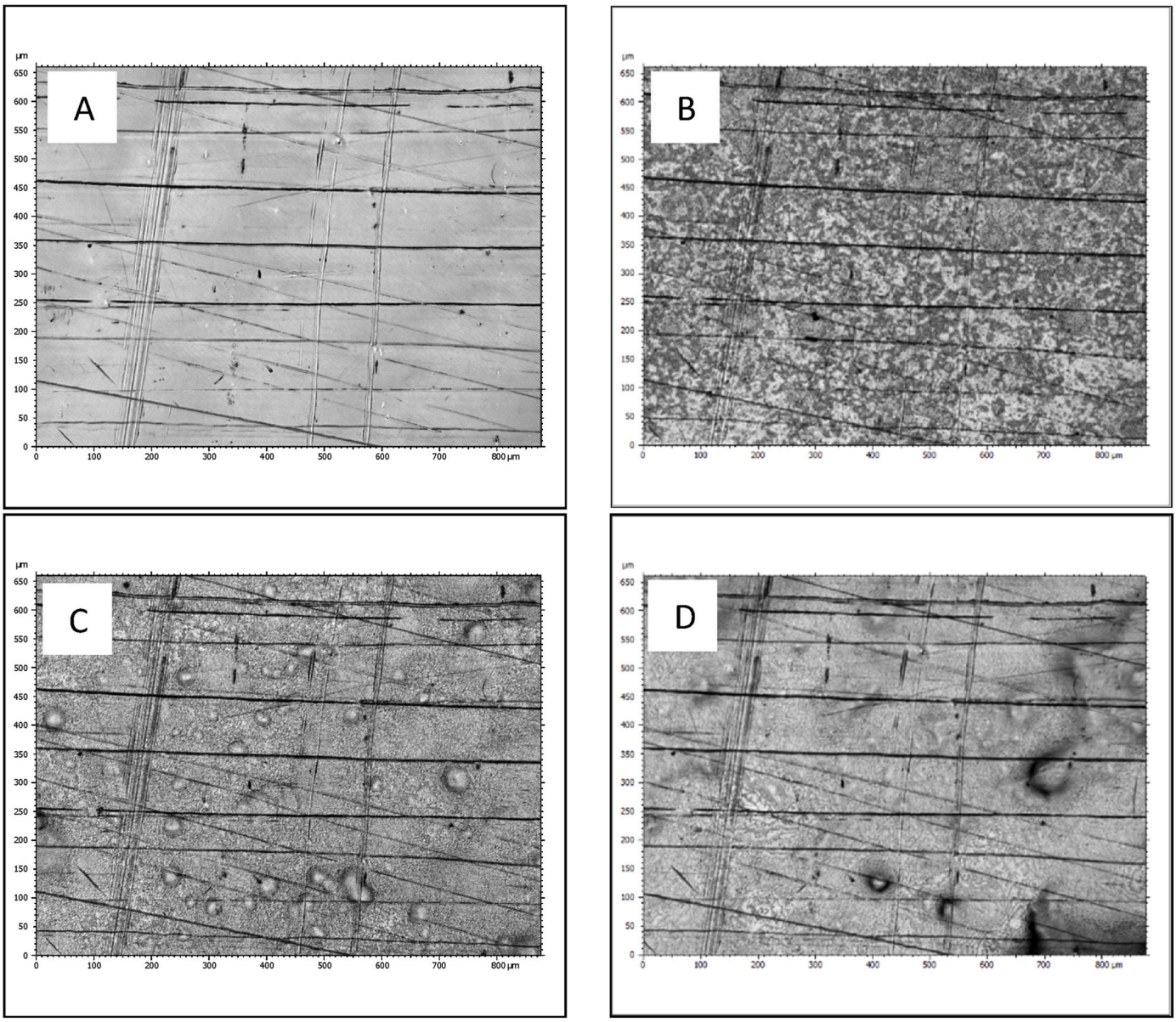

Fig. 10. Images of stainless steel electropolished (EP SS316L) coupons. (A) Clean EP SS316L surface. Biofilm-coated surfaces at different incubation periods of (B) 24 h, (C) 48 h and (D) 72 h, magnification 20×, area (850 × 650) μm^2.

Table 1
Biofilm coverage area (%) and roughness of uncoated and biofilm-coated EP SS316L surfaces at different incubation times[a].

Incubation time (h)	Biofilm Coverage Area (%)	SD (%)	Roughness, SDR (%)	SD (%)	Net Maximum height, Sz (µm)	Net Root mean square height, Sq (µm)
Clean surface	0.00	0.0	0.038	0.012	0	0
24	49.59	4.8	0.061	0.012	0.11	0.01
48	99.00	1.0	0.094	0.023	1.31	0.23
72	100.00	0.0	0.121	0.055	2.73	0.29

[a]Calculations are performed in triplicate.

preventing environmental and human health hazards.

Author contributions statement

Zoi Christina Kampouraki: Conceptualization, Methodology, Validation, Formal analysis, Investigation, Data Curation, Writing - Original Draft, Visualization, **Maria Petala:** Conceptualization, Methodology, Validation, Investigation, Data Curation, Writing - Original Draft, Writing - Review & Editing, Visualization, **Konstantinos Zacharias:** Conceptualization, Methodology, Software, Validation, Formal analysis, Investigation, Data Curation, Writing - Review & Editing, **Avraam Konstantinidis:** Validation, Writing - Review & Editing, **Xenophon Zabulis**: Software, Formal analysis, **Polykarpos Karamaounas**: Software, Formal analysis, **Margaritis Kostoglou:** Validation, Writing - Review & Editing, Supervision, **Thodoris D. Karapantsios:** Conceptualization, Methodology, Validation, Resources, Writing - Review & Editing, Supervision, Project administration, Funding acquisition.

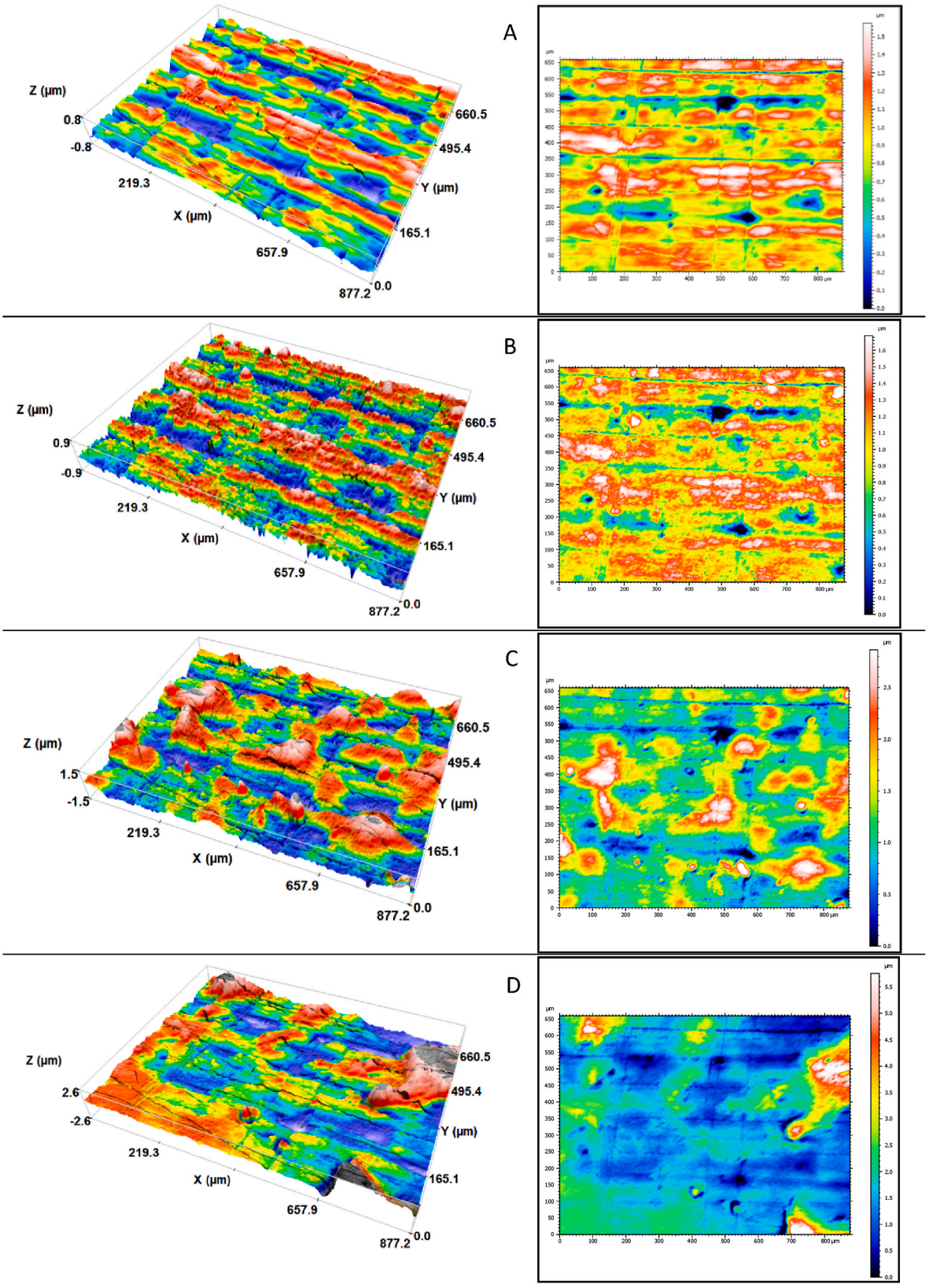

Fig. 11. Profilometric images of biofilms grown under laminar flow at incubation times of: (A) 0 h, (B) 24 h, (C) 48 h, (D) 72 h, magnification 20×, area (850 × 650) μm^2.

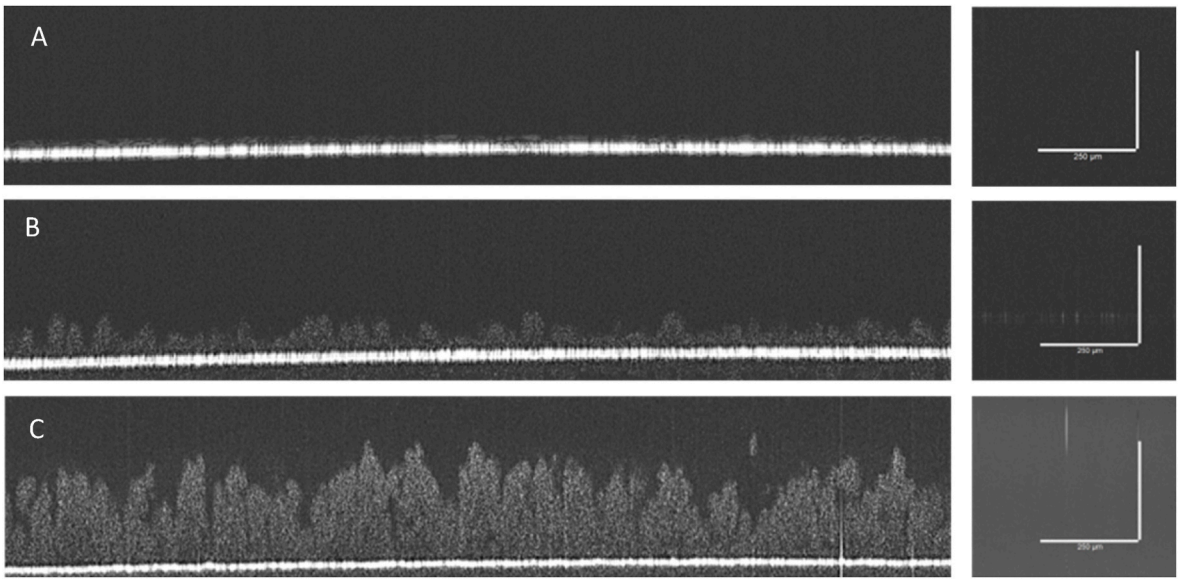

Fig. 12. OCT images captured on SSEP316L biofilm surfaces after 24, 48 and 72 h.

Declaration of competing interest

The authors declare that they have no known competing financial interests or personal relationships that could have appeared to influence the work reported in this paper.

Data availability

No data was used for the research described in the article.

Acknowledgment

This study was conducted under the umbrella of the European Space Agency Topical Team: Biofilms from an Interdisciplinary Perspective and supported financially by Helleniq Energy.

Appendix A. Supplementary data

Supplementary data to this article can be found online at https://doi.org/10.1016/j.envres.2023.117401.

References

Adetunji, V., Odetokun, I., 2012. Assessment of biofilm in E. coli O157:H7 and Salmonella strains: influence of cultural conditions. Am. J. Food Technol. 7, 582–595. https://doi.org/10.3923/ajft.2012.582.595.

Asséré, A., Oulahal, N., Carpentier, B., 2008. Comparative evaluation of methods for counting surviving biofilm cells adhering to a polyvinyl chloride surface exposed to chlorine or drying. J. Appl. Microbiol. 104, 1692–1702. https://doi.org/10.1111/j.1365-2672.2007.03711.x.

Bayoudh, S., Othmane, A., Ponsonnet, L., Ben Ouada, H., 2008. Electrical detection and characterization of bacterial adhesion using electrochemical impedance spectroscopy-based flow chamber. Colloids Surfaces A Physicochem. Eng. Asp. 318, 291–300. https://doi.org/10.1016/j.colsurfa.2008.01.005.

Beech, I.B., Sunner, J., 2004. Biocorrosion: towards understanding interactions between biofilms and metals. Curr. Opin. Biotechnol. 15, 181–186. https://doi.org/10.1016/j.copbio.2004.05.001.

Bruchmann, J., Sachsenheimer, K., Rapp, B.E., Schwartz, T., 2015. Multi-channel microfluidic biosensor platform applied for online monitoring and screening of biofilm formation and activity. PLoS One 10, 1–19. https://doi.org/10.1371/journal.pone.0117300.

Castigliano, M., Recupido, F., Petala, M., Kostoglou, M., Caserta, S., Karapantsios, T.D., 2021. Wetting of dehydrated hydrophilic Pseudomonas fluorescens biofilms under the action of external body forces. Langmuir 37, 10890–10901. https://doi.org/10.1021/acs.langmuir.1c00528.

Ceri, H., Olson, M.E., Stremick, C., Read, R.R., Morck, D., Buret, A., 1999. The Calgary biofilm device: new technology for rapid determination of antibiotic susceptibilities of bacterial biofilms. J. Clin. Microbiol. 37, 1771–1776. https://doi.org/10.1128/jcm.37.6.1771-1776.1999.

Chabowski, K., Junka, A.F., Szymczyk, P., Piasecki, T., Sierakowski, A., Mączyńska, B., Nitsch, K., 2015. The application of impedance microsensors for real-time analysis of Pseudomonas aeruginosa biofilm formation. Pol. J. Microbiol. 64, 115–120. https://doi.org/10.33073/pjm-2015-017.

Chatterjee, S., Biswas, N., Datta, A., Dey, R., Maiti, P., 2014. Atomic force microscopy in biofilm study. Microscopy 63, 269–278. https://doi.org/10.1093/jmicro/dfu013.

Chen, M.Y., Chen, M.J., Lee, P.F., Cheng, L.H., Huang, L.J., Lai, C.H., Huang, K.H., 2010. Towards real-time observation of conditioning film and early biofilm formation under laminar flow conditions using a quartz crystal microbalance. Biochem. Eng. J. 53, 121–130. https://doi.org/10.1016/j.bej.2010.10.003.

Cloete, E., Molobela, I., Van Der Merwe, A., Richards, M., 2009. Biofilms in the food and beverage industries: an introduction. Biofilms Food Beverage Ind 3–41. https://doi.org/10.1533/9781845697167.1.3.

Costerton, J.W., 1999. Introduction to biofilm. Int. J. Antimicrob. Agents 11, 217–221. https://doi.org/10.1016/S0924-8579(99)00018-7.

Costerton, J.W., Stewart, P.S., Greenberg, E.P., 1999. Bacterial biofilms: a common cause of persistent infections. Science 284, 1318–1322. https://doi.org/10.1126/science.284.5418.1318.

European Centre for Disease Prevention and Control-European Medicines Agency, 2009. The Bacterial Challenge: Time to React – A Call to Narrow the Gap between Multidrug-Resistant Bacteria in the EU and the Development of New Antibacterial Agents. Stockholm.

Evgenidis, S., Karapantsios, T., 2022. Pulsatile gas-liquid flow resembling Decompression Sickness: computational Fluid Dynamics simulation and experimental validation. Int. Marit. Health 73, 189–198. https://doi.org/10.5603/IMH.2022.0033.

Evgenidis, S.P., Karapantsios, T.D., 2015. Effect of bubble size on void fraction fluctuations in dispersed bubble flows. Int. J. Multiphas. Flow 75, 163–173. https://doi.org/10.1016/j.ijmultiphaseflow.2015.05.013.

Furst, A.L., Francis, M.B., 2019. Impedance-based detection of bacteria. Chem. Rev. 119, 700–726. https://doi.org/10.1021/acs.chemrev.8b00381.

Gamal, W., Wu, H., Underwood, I., Jia, J., Smith, S., Bagnaninchi, P.O., 2018. Impedance-based cellular assays for regenerative medicine. Philos. Trans. R. Soc. B Biol. Sci. 373, 1–8. https://doi.org/10.1098/rstb.2017.0226.

Giaever, I., Keese, C.R., 1993. A morphological biosensor for mammalian cells. Nature 366, 591–592. https://doi.org/10.1038/366591a0.

Gkotsis, P.K., Evgenidis, S.P., Karapantsios, T.D., 2020. Associating void fraction signals with bubble clusters features in co-current, upward gas-liquid flow of a non-Newtonian liquid. Int. J. Multiphas. Flow 131, 103297. https://doi.org/10.1016/j.ijmultiphaseflow.2020.103297.

Guła, G., Szymanowska, P., Piasecki, T., Góras, S., Gotszalk, T., Drulis-Kawa, Z., 2020. The application of impedance spectroscopy for Pseudomonas biofilm monitoring during phage infection. Viruses 12, 1–19. https://doi.org/10.3390/v12040407.

Hall-Stoodley, L., Costerton, J.W., Stoodley, P., 2004. Bacterial biofilms: from the natural environment to infectious diseases. Nat. Rev. Microbiol. 2, 95–108. https://doi.org/10.1038/nrmicro821.

International Organisation for Standardization, 2012. ISO 25178. Geometrical Product Specifications (GPS) – Surface Texture: Area – Part 2: Terms, Definitions and Surface Texture Parameters.

Kampouraki, Z.C., Petala, M., Boumpakis, A., Skordaris, G., Michailidis, N., Deliyanni, E., Kostoglou, M., Karapantsios, T.D., 2022. Wetting and imbibition characteristics of Pseudomonas fluorescens biofilms grown on stainless steel. Langmuir 38, 9810–9821. https://doi.org/10.1021/acs.langmuir.2c00828.

Karapantsios, T., Evgenidis, S., Zacharias, K., Karagiannis, G., 2017. Non-invasive Impedance Spectroscopy Device for Early Diagnosis of Coronary Artery Disease and Method Therefor. European Patent Office, EP 3245947 A1.

Karapantsios, T., Evgenidis, S., Zacharias, K., Mesimeris, T., 2016. Method for the Detection and Characterization of Bubbles in Liquids and Device Therefor, Resp. System. European Patent Office, EP 3005942 A1.

Kim, T., Kang, J., Lee, J.H., Yoon, J., 2011. Influence of attached bacteria and biofilm on double-layer capacitance during biofilm monitoring by electrochemical impedance spectroscopy. Water Res. 45, 4615–4622. https://doi.org/10.1016/j.watres.2011.06.010.

LeChevallier, M.W., Babcock, T.M., Lee, R.G., 1987. Examination and characterization of distribution system biofilms. Appl. Environ. Microbiol. 53, 2714–2724. https://doi.org/10.1128/aem.53.12.2714-2724.1987.

Liu, S., Gunawan, C., Barraud, N., Rice, S.A., Harry, E.J., Amal, R., 2016. Understanding, monitoring, and controlling biofilm growth in drinking water distribution systems. Environ. Sci. Technol. 50, 8954–8976. https://doi.org/10.1021/acs.est.6b00835.

Magar, H.S., Hassan, R.Y.A., Mulchandani, A., 2021. Electrochemical impedance spectroscopy (EIS): principles, construction, and biosensing applications. Sensors 21, 1–21. https://doi.org/10.3390/s21196578.

Marra, D., Recupido, F., Toscano, G., Caserta, S., 2022. Bacterial motility in biofilm under shear flow. Chem. Eng. Trans. 93, 325–330. https://doi.org/10.3303/CET2293055.

Martínez-García, P.M., Ruano-Rosa, D., Schilirò, E., Prieto, P., Ramos, C., Rodríguez-Palenzuela, P., Mercado-Blanco, J., 2015. Complete genome sequence of Pseudomonas fluorescens strain PICF7, an indigenous root endophyte from olive (Olea europaea L.) and effective biocontrol agent against Verticillium dahliae. Stand. Genomic Sci. 10, 1–7. https://doi.org/10.1186/1944-3277-10-10.

McCutcheon, J., Southam, G., 2018. Advanced biofilm staining techniques for TEM and SEM in geomicrobiology: implications for visualizing EPS architecture, mineral nucleation, and microfossil generation. Chem. Geol. 498, 115–127. https://doi.org/10.1016/j.chemgeo.2018.09.016.

Moradi, M., Ghiara, G., Spotorno, R., Xu, D., Cristiani, P., 2022. Understanding biofilm impact on electrochemical impedance spectroscopy analyses in microbial corrosion and microbial corrosion inhibition phenomena. Electrochim. Acta 426, 140803. https://doi.org/10.1016/j.electacta.2022.140803.

Munson, B., Young, D., Okiishi, T., 1990. Viscous flow in pipes. In: Fundamentals of Fluid Mechanics. John Wiley and Sons, New York, pp. 465–559.

Nakagawa, R., Saito, K., Kanematsu, H., Miura, H., Ishihara, M., Barry, D.M., Kogo, T., Ogawa, A., Hirai, N., Hagio, T., Ichino, R., Ban, M., Yoshitake, M., Zimmermann, S., 2022. Impedance characteristics of monolayer and bilayer graphene films with biofilm formation and growth. Sensors 22, 1–11. https://doi.org/10.3390/s22093548.

Oikonomidou, O., Evgenidis, S.P., Kostoglou, M., Karapantsios, T.D., 2018. Degassing of a pressurized liquid saturated with dissolved gas when injected to a low pressure liquid pool. Exp. Therm. Fluid Sci. 96, 347–357. https://doi.org/10.1016/j.expthermflusci.2018.03.018.

Olsson, A.L.J., Mitzel, M.R., Tufenkji, N., 2015. QCM-D for non-destructive real-time assessment of Pseudomonas aeruginosa biofilm attachment to the substratum during biofilm growth. Colloids Surf. B Biointerfaces 136, 928–934. https://doi.org/10.1016/j.colsurfb.2015.10.032.

Paredes, J., Becerro, S., Arizti, F., Aguinaga, A., Del Pozo, J.L., Arana, S., 2013. Interdigitated microelectrode biosensor for bacterial biofilm growth monitoring by impedance spectroscopy technique in 96-well microtiter plates. Sens. Actuators, B 178, 663–670. https://doi.org/10.1016/j.snb.2013.01.027.

Paredes, J., Becerro, S., Arizti, F., Aguinaga, A., Del Pozo, J.L., Arana, S., 2012. Real time monitoring of the impedance characteristics of Staphylococcal bacterial biofilm cultures with a modified CDC reactor system. Biosens. Bioelectron. 38, 226–232. https://doi.org/10.1016/j.bios.2012.05.027.

Petala, M., Tsiridis, V., Mintsouli, I., Pliatsikas, N., Spanos, T., Rebeyre, P., Darakas, E., Patsalas, P., Vourlias, G., Kostoglou, M., Sotiropoulos, S., Karapantsios, T., 2017. Silver deposition on stainless steel container surfaces in contact with disinfectant silver aqueous solutions. Appl. Surf. Sci. 396, 1067–1075. https://doi.org/10.1016/j.apsusc.2016.11.090.

Prest, E.I., Hammes, F., van Loosdrecht, M.C.M., Vrouwenvelder, J.S., 2016. Biological stability of drinking water: controlling factors, methods, and challenges. Front. Microbiol. 7, 1–24. https://doi.org/10.3389/fmicb.2016.00045.

Roßteuscher, T., 2009. Online Monitoring of Biofilm in Microchannels with Thermal Lens Microscopy. Technische Universität München.

Scales, B.S., Dickson, R.P., Lipuma, J.J., Huffnagle, G.B., 2014. Microbiology, genomics, and clinical significance of the Pseudomonas fluorescens species complex, an unappreciated colonizer of humans. Clin. Microbiol. Rev. 27, 927–948. https://doi.org/10.1128/CMR.00044-14.

Schlafer, S., Meyer, R.L., 2017. Confocal microscopy imaging of the biofilm matrix. J. Microbiol. Methods 138, 50–59. https://doi.org/10.1016/j.mimet.2016.03.002.

Song, J., Li, Y., Yin, F., Zhang, Z., Ke, D., Wang, D., Zhang, X.E., Yuan, Q., 2020. Enhanced electrochemical impedance spectroscopy analysis of microbial biofilms on an electrochemically in situ generated graphene interface. ACS Sens. 5, 1795–1803. https://doi.org/10.1021/acssensors.0c00570.

Turolla, A., Di Mauro, M., Mezzera, L., Antonelli, M., Carminati, M., 2019. Development of a miniaturized and selective impedance sensor for real-time slime monitoring in pipes and tanks. Sens. Actuators, B 281, 288–295. https://doi.org/10.1016/j.snb.2018.10.107.

Tzevelecos, W., Galand, Q., Evgenidis, S., Zacharias, K., Karapantsios, T., Van Vaerenbergh, S., 2021. High-resolution concentration measurement in water/n-butanol binary system by means of high-frequency electrical impedance method. Exp. Therm. Fluid Sci. 126, 110399 https://doi.org/10.1016/j.expthermflusci.2021.110399.

WHO, 2002. Global Meeting on the Revision of WHO Guidelines for Drinking-Water Quality. Tokyo, Japan.

Wilson, C., Lukowicz, R., Merchant, S., Valquier-Flynn, H., Caballero, J., Sandoval, J., Okuom, M., Huber, C., Brooks, T.D., Wilson, E., Clement, B., Wentworth, C.D., Holmes, A.E., 2017. Quantitative and qualitative assessment methods for biofilm growth: a mini-review Christina. Res Rev J Eng Technol 6, 1–42.

Yin, W., Wang, Y., Liu, L., He, J., 2019. Biofilms: the microbial “protective clothing” in extreme environments. Int. J. Mol. Sci. 20, 1–18. https://doi.org/10.3390/ijms20143423.